Time-Resolved CRDS Measurements of the $N_2(A^3\Sigma_u^+)$ Density Produced by Nanosecond Discharges in Atmospheric Pressure Nitrogen and Air

Gabi D. Stancu,* Mario Janda,† Farah Kaddouri, Deanna A. Lacoste, and Christophe O. Laux

Laboratoire EM2C, CNRS UPR 288, Ecole Centrale Paris, Châtenay-Malabry, 92295 Cedex, France

Received: August 5, 2009; Revised Manuscript Received: October 8, 2009

Cavity ring-down spectroscopy (CRDS) is used to measure the number density of $N_2(A^3\Sigma_u^+)$ metastables produced by nanosecond repetitively pulsed discharges in nitrogen and air preheated at 1000 K and atmospheric pressure. The densities of $N_2(A)$ are inferred from the absorbance of the $Q_1(22)$ and $Q_3(16)$ lines of the $(2 \leftarrow 0)$ vibrational band of the first positive system ($B^3\Pi_g - A^3\Sigma_u^+$) of N_2 at 769.945 nm. The procedure for determining the temporal evolution of the density of metastable from the measured ring down signals is presented. The maximum number densities are in the range of $10^{14}-10^{15}$ molecules cm^{-3} for air and nitrogen discharges, respectively. In nitrogen, the decay of the $N_2(A)$ density is shown to be a second-order process with a rate coefficient of 1.1×10^{-9} cm^3 s^{-1} at 1600 K with a factor of 2 uncertainty. In air, the decay is estimated to be 1 order of magnitude faster than that in nitrogen owing to quenching by atomic and molecular oxygen. Furthermore, the rotational temperature is determined by comparison of CRDS measurements and simulations of several rotational lines of the $(2 \leftarrow 0)$ band of the first positive system of N_2 between 769.8 and 770.7 nm. The rotational and vibrational temperatures are also determined by comparison of optical emission measurements and simulations of the second positive system of N_2 between 365 and 385 nm. In these CRDS measurements, we achieved a temporal resolution down to 50 ns.

1. Introduction

Atmospheric pressure air- or nitrogen-containing plasmas are increasingly used for surface treatment, gas purification, aerodynamic flow control, plasma-assisted combustion, or destruction of toxic compounds.[1] The efficiency of these processes depends on the amount of active species produced, which itself strongly depends on the plasma sources employed. Here, we use a nanosecond repetitively pulsed (NRP) discharge generated between two pin electrodes, a promising plasma generation technique owing to its very low power requirements in comparison with traditional dc, rf, or microwave discharges.[2,3] With pulses of 10 ns duration and electric fields of about 10 kV/cm, NRP discharges can operate in the filamentary mode or in the diffuse mode.[4] Here, we study a filamentary discharge in nitrogen or air preheated to a temperature of 1000 K. With the electric fields considered, the NRP discharge produces a nonthermal plasma with a peak electron density of the order of 10^{15} cm^{-3} and an electron temperature[2] of the order of $2 \times 10^4 - 5 \times 10^4$ K, well above the gas temperature of 1000 K. The gas temperature of 1000 K was used because it is representative of conditions of low temperature flames and exhaust gas treatment, thus allowing for investigations of plasma chemistry in such environments.

One of the active species produced in nitrogen or air discharges is the first excited electronic state $A^3\Sigma_u^+$ of molecular nitrogen. It plays an important role in air or nitrogen chemical reactors, for instance in NO formation,[5,6] but also in the Earth's atmosphere. Often termed metastable N_2 because of its long radiative lifetime of the order of seconds, $N_2(A)$ is a reservoir of energy for chemical processes. For example, the excitation energy of this state ($E_{ex} = 6.2$ eV) is sufficient to dissociate molecular oxygen ($E_{dis} = 5.1$ eV) and thus produce atomic oxygen radicals.

In electrical discharges, $N_2(A)$ is produced mainly by electron-impact excitation of ground state nitrogen and additionally by radiative cascade from higher electronic states, e.g., $N_2(C) \rightarrow N_2(B) \rightarrow N_2(A)$. At atmospheric pressure $N_2(A)$ can also be produced by collisional quenching of high electronic states such as $N_2(B)$ or $N_2(C)$.

The main mechanism of depletion of $N_2(A)$ is through quenching reactions such as

$$N_2(A) + \text{atom, molecule} \rightarrow \text{products} \qquad \text{(R1)}$$

whose rates strongly depend on the type and densities of the species present in the plasma. References 7−11 report the quenching rates with H, O, OH, NO, O_2, CH_3CN, and hydrogen and methyl halides measured with discharge flow techniques at room temperature and low pressure. Vibrational-level-dependent (up to $v = 7$) quenching rates of $N_2(A)$ by O_2, NO, and O were measured by De Benedictis et al.[11] at $P = 0.1$ Torr and $T = 340$ K. The temperature dependence of the quenching rates by O_2, between 80 and 560 K, was measured by De Sousa et al.[8] at a pressure of 0.4 Torr.

Another possible depletion mechanism is via energy pooling reactions such as

$$N_2(A,v) + N_2(A,v) \rightarrow N_2(X) + N_2^* \qquad \text{(R2)}$$

where N_2^* is one of the following states: $N_2(B)$, $N_2(C)$, $N_2(C')$, N_2(HIR) (upper state of Herman infrared system). References 12−16 report the pooling rates for different excitation channels. A total pooling rate in the range of 3×10^{-10} to 3×10^{-9} cm^3 s^{-1} was obtained. These values were measured in a room temperature, low-pressure afterglow apparatus. The large value of the pooling rate reduces the metastable potential as a source of production of excited atoms and molecules.

* Author to whom the correspondence should be addressed, stancu@em2c.ecp.fr.

† Present address: Comenius University, Bratislava, Slovakia.

10.1021/jp9075383 © 2010 American Chemical Society
Published on Web 12/03/2009

However, at atmospheric pressure and elevated gas temperatures, the mechanism of deactivation and the depletion rates of $N_2(A)$ state are still uncertain. Yet, these conditions are of interest for applications such as plasma-assisted combustion.[17] In such applications, it has been proposed that the exothermic dissociative quenching with molecular oxygen ($N_2(A,B,C) + O_2 \rightarrow N_2(X) + 2\ O$) may be one of the key paths for the formation of atomic oxygen; see for instance[18] and references therein. The large quantities of atomic oxygen thus produced would increase the rate of fuel oxidation, thus promoting and stabilizing combustion in lean flames which are less polluting.

To prove this mechanism, the densities of $N_2(A)$ metastable, $N_2(B)$, $N_2(C)$, and the density of atomic oxygen must be measured simultaneously. The measurements of $N_2(A)$ are particularly challenging because the small plasma volume ($1-5$ mm^3) and short lifetime of the metastable species (10 ns-1 μs) at atmospheric pressure drastically limit the diagnostic techniques available. In this paper, we address the detection by CRDS of $N_2(A)$ at atmospheric pressure in air or nitrogen preheated to 1000 K. The depletion mechanisms of the metastable in the postdischarge are discussed. The detection of atomic oxygen and of the excited electronic states of N_2 will be reported in a forthcoming paper.

In the following sections, we first review the diagnostic techniques that can be applied to the detection of $N_2(A)$, then we present the CRDS technique used in the present work for time-resolved measurements of this species in air or nitrogen NRP discharges, the rotational and vibrational temperature measurements, and we end with a discussion of the depletion mechanisms of the metastable present in these environments.

Overview of $N_2(A)$ Detection Techniques. The detection of $N_2(A)$ has been the subject of many articles. One possibility is to measure $N_2(A)$ by emission spectroscopy using the Vegard−Kaplan (VK) band system ($A^3\Sigma_u^+ \rightarrow X^1\Sigma_g^+$). However, this spin-forbidden transition being very weak, its detection is only possible under special conditions such as those of the low pressure afterglow[8,14] in which the lifetime of the metastable state is sufficiently long. Under such conditions, measurements can be made in the spectral region 200−460 nm corresponding to transitions from the excited $N_2(A)$, $v = 0, 1, 2, 3$ to the ground state $N_2(X)$, $v = 0, .., 15$. At atmospheric pressure, however, the detection of the VK band system is not possible owing to fast quenching and to the overlap with the intense second positive system of N_2 ($C \rightarrow B$) and the gamma system of NO ($A \rightarrow X$).

Another possible technique for the measurement of $N_2(A)$ densities is laser-induced fluorescence (LIF)[11,19,20] which consists in pumping the $N_2(B,v') \leftarrow N_2(A,v')$ transition and detecting the fluorescence of the first positive system of N_2 ($B \rightarrow A$). Enhanced sensitivity is achieved using optical−optical double resonance (OODR) LIF,[21] by further pumping the $N_2(C,v''') \leftarrow N_2(B,v')$ transition using a second laser and detecting the fluorescence of the second positive system of N_2 ($C \rightarrow B$), which has a higher transition probability by about 3 orders of magnitude. This method has the advantages of high sensitivity (in ref 20, de Benedictis et al. were able to detect $N_2(A)$ down to a minimum level of 10^{11} cm^{-3}) and high time resolution (limited by the laser temporal width), but the disadvantages are the complex calibration procedure and difficulties on defining the lower state for the LIF process.

Laser optogalvanic spectroscopy (OGS) has been proposed by Hadj Bachir et al.[22] Although the technique provides high-resolution spectra, it requires a complex calibration procedure and is intrusive in nature owing to the presence of electrodes.

$N_2(A)$ was also measured by absorption spectroscopy of the first positive system using lamps or plasmas as resonant sources of light.[23] Scripter el al. and Augustyniak et al.[24,25] used high-resolution tunable diode laser absorption spectroscopy (TDLAS with a 10 MHz laser line width). These authors measured the absorption profiles of the $O_{12}(22)$ and $O_{12}(16)$ lines of the (2,0) band and of the $R_3(22)$ line of the (7,6) band in the region 777.668−777.683 nm. The sensitivity had to be enhanced by employing multipass techniques (absorption length of 1.2 m) in a large volume of metastable molecules.

For our experimental conditions, none of the above techniques are adequate. The discharge HV electrodes do not allow for the insertion of an additional electrode as used in the optogalvanic experiments. The low expected $N_2(A)$ densities (10^{14} cm^{-3}), the small spatial scales (sub-mm), and the fast varying densities (species lifetime sub-μs) due to high quenching and pooling rates at atmospheric pressure require a highly sensitive and temporally resolved technique; thus TDLAS is not well suited.

For these reasons, we resorted to cavity ring-down spectroscopy (CRDS), which was used here for the first time to measure $N_2(A)$ densities by probing the $B \leftarrow A$ transition (first positive system) around 770 nm with a pulsed dye laser. The pulsed CRDS technique[26] can typically resolve absorbances down to 10^{-6}. Compared with the techniques previously mentioned, CRDS offers high sensitivity and high temporal resolution and does not require calibration.

In the following section, we present the CRDS technique and the procedure to infer time-resolved $N_2(A)$ densities from the CRDS data.

2. Theory

The CRDS technique has been used for the detection of many species in plasmas.[27−29] A detailed overview of the principles and applicability of this technique can be found in ref 29. Much less has been published for time-resolved measurements using CRDS.[30,31] Thus we start by briefly describing the technique and data analysis procedure for time-resolved measurements.

In pulsed CRDS, a laser pulse is coupled into an optical cavity formed by two high reflectivity mirrors. Each time the pulse reaches one of the mirrors, a small fraction of the light leaks out. At the exit of the cavity a train of pulses decaying in time can be recorded with a photomultiplier tube (PMT). When the laser is tuned to an absorption transition of the species present inside the cavity, the decay of pulses is faster. The difference of the decay times for on- and off-resonance measurements is proportional to the absorbing species density.

The loss-per-path, ΔI, of the light intensity, I, inside the cavity has two main causes, the absorption loss due to the gas sample and the transmission loss through one cavity mirror. The value of ΔI is given by

$$\Delta I = -[k(\nu)l_{abs} + (1 - R)]I \qquad (1)$$

where $k(\nu)$ is the absorption coefficient, l_{abs} is the length of the absorption volume, and R is the reflectivity of the mirrors.

If the absorbance per path, defined as $A(\nu) = k(\nu)l_{abs}$, is much smaller than unity (typical absorbances in pulsed CRDS experiments are $10^{-3}-10^{-6}$) and if the mirror transmissivity is very low (typical mirror transmissivities in CRDS experiments are $T = 1 - R < 10^{-3}$), then the loss-per-path is negligibly small in comparison with the loss over the complete ring-down signal decay that is measured over a few thousand paths. Typically, the path time is of the order of nanoseconds while the decay time is of the order of microseconds to milliseconds.

Thus the ring-down decay signal can be discretized in units of loss-per-path. The loss per unit length is then differentially given by

$$\frac{dI}{dl} = -\frac{[k(\nu)l_{abs} + (1 - R)]I}{L} \quad (2)$$

where L is the length of the cavity. If the cavity is not used and if $L = l_{abs}$, the classical Beer−Lambert law is recovered by integrating eq 2

$$I(\nu) = I_0(\nu) \exp[-k(\nu)l_{abs}] \quad (3)$$

where $I(\nu)$ is the transmitted light through a homogeneous absorbing medium of length l_{abs}, and $I_0(\nu)$ is the incident light. The resulting absorption coefficient, $k(\nu)$, is given by

$$k(\nu) = \frac{1}{l_{abs}} \ln\left(\frac{I_0}{I}\right)_\nu \quad (4)$$

where $\ln(I_0/I)_\nu = A(\nu)$ is the absorbance.

The absorption coefficient is related to the species number density, N, of the absorbing species by

$$k(\nu) = \sum_i (S_i(T)\phi_i(\nu))N \quad (5)$$

where the summation runs over all lines i that contribute to the measured spectrum, $S_i(T)$ is the line strength of line i at temperature T, and $\phi_i(\nu)$ is the Voigt absorption line shape normalized to 1 ($\int\phi(\nu)\, d\nu = 1$) and accounting for natural, Doppler, van der Waals, resonance, and instrumental broadening. Thus, if the absorption coefficient is measured and the line strengths are known, absolute species densities are obtained.

If no absorber is present inside the cavity ($k(\nu) = 0$), by substituting $dl = c\, dt$ (c is the speed of light) in (2) and integrating, the classical empty-cavity ring-down intensity, I_1, is obtained as

$$I_1(t) = I_0 \exp\left[-\frac{c}{L}(1 - R)t\right] \quad (6)$$

When an absorbing species of uniform, constant density is introduced inside the cavity, the ring-down intensity I_2 obtained by integrating eq 2 is

$$I_2(t) = I_0 \exp\left\{-\frac{c}{L}[(1 - R) + k(\nu)l_{abs}]t\right\} \quad (7)$$

The ring-down expressions given by eqs 6 and 7 are well-known results.[26] They represent the typical single exponential CRDS decay signals. The corresponding decay times (the time for which the intensity is I_0/e) for the empty and absorbing sample cavities are noted τ_{empty} and τ_{abs}, respectively, and have the following expressions

$$\tau_{empty} = \frac{L}{c(1 - R)} \quad (8)$$

$$\tau_{abs} = \frac{L}{c[(1 - R) + k(\nu)l_{abs}]} \quad (9)$$

Combining eqs 8 and 9, the absorption coefficient is obtained as

$$k(\nu) = \frac{L}{cl_{abs}}\left(\frac{1}{\tau_{abs}} - \frac{1}{\tau_{empty}}\right) \quad (10)$$

The absorbing species density can then be deduced with the help of eq 5 and the measured decay times τ_{empty} and τ_{abs}. However, scattering, beam steering losses, or background absorption of other species may affect the ring-down signals.

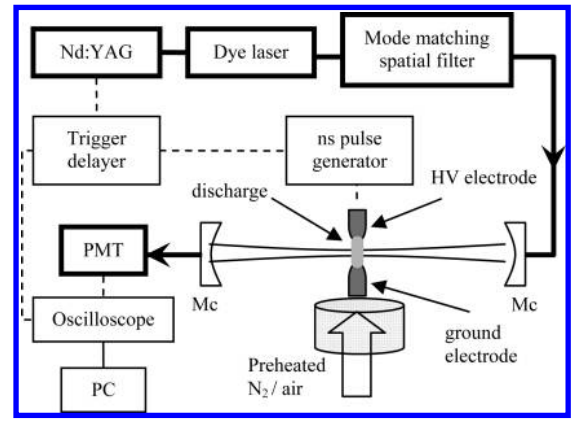

Figure 1. Schematic of the atmospheric pressure nanosecond repetitively pulsed discharge with CRDS experimental setup (Mc, cavity mirror).

In practice, rather than measuring the decay time difference of the empty and filled cavities, one considers the difference of the on- and off-resonance signals.

If the density of the absorber changes during the ring-down time, the absorption coefficient becomes a function of time, $k(\nu,t)$. As shown in ref 30, the ring-down signal, $I_3(t)$, can then be expressed by time-integrating the absorption loss in eq 7

$$I_3(t) = I_0 \exp\left\{-\frac{c}{L}[(1 - R)t + \int_0^t k(\nu, t)l_{abs}\, dt]\right\} \quad (11)$$

Combining eqs 6 and 11, the time-dependent absorption coefficient is obtained as

$$k(\nu, t) = \frac{L}{cl_{abs}}\frac{d}{dt}\left(\ln\frac{I_1}{I_3}\right) \quad (12)$$

From eqs 5 and 12 the time evolution of the species density is given by

$$N(t) = \frac{1}{\sum_i (S_i(T)\phi_i(\nu))}\frac{L}{cl_{abs}}\frac{d}{dt}\left(\ln\frac{I_1}{I_3}\right) \quad (13)$$

3. Experimental Section

Nanosecond repetitively pulsed discharges were generated in atmospheric pressure air or nitrogen, preheated to 1000 K and flowing at velocities in the range of 1−2 m/s. The discharges were produced with high-voltage pulses of 10 ns duration, 5−8 kV amplitude, and pulse repetition frequencies of 10 kHz. The high-voltage pulses were produced by a solid-state generator (FID Technologies FPG 10-30MS) that generates pulses with rise/fall times of about 5 ns, and a flat top of 10 ns at greater than 90% of the maximum voltage. The voltage pulses were applied between two pin electrodes separated by a distance of 4 mm.

A schematic of the CRDS setup and of the atmospheric pressure nitrogen/air discharge is shown in Figure 1. The CRDS cavity consists of two plano-concave mirrors (Los Gatos Research) of high reflectivity, $R > 99.97\%$, and radius of curvature $r = 0.5$ m. The beam of a tunable pulsed dye laser, Continuum ND 6000, pumped with a Precision PL 8010 Nd:YAG laser was coupled into the cavity. The output laser energy per pulse was up to 40 mJ at 770 nm, the laser spectral width was 0.1 cm^{-1}, and the repetition frequency was 10 Hz.

The density of $N_2(A)$ was determined by probing the (2 ← 0) vibrational band of the N_2 first positive system (B ← A) in the vicinity of 770 nm. This spectral region was chosen because it contains some of the strongest absorption lines and it accesses $N_2(A, v = 0)$ density. The dye laser output sent to the cavity was attenuated down to a few hundred microjoules per pulse by reducing the power of the Nd:YAG laser. The light leaking out of the cavity was filtered by two interferential bandpass filters (CVI-F10-770) with peak transmittance at 770 nm and a band transmissivity of 10 nm (fwhm, full width at half-maximum). It was then focused into a 5 m long optical fiber and transmitted to a photomultiplier tube (PMT) with 1.4 ns rise time (Hamamatsu H9305-3). The PMT signal was digitized by a LeCroy Waverunner 434 oscilloscope (350 MHz analog bandwidth, eight-bit vertical resolution) and recorded by a computer under Labview. Faraday cages were used to shield the PMT system from the electromagnetic noise produced by the pulsed discharge equipment.

The plasma discharge, laser system, and detection system were synchronized by a Berkeley Nucleonics (BNC) 555 four-channel gate and delay generator. The BNC triggered the flash lamp and Q-switch of the Nd:YAG laser and the detection system at 10 Hz and the discharge at 10 kHz with appropriate delays. For density measurements 100 decay curves were averaged at on- and off-resonance wavelengths. Spectral scans were acquired at wavelength steps of 5 pm, and spatial scans were taken with steps of 0.1 mm across the diameter of the discharge. The profile of measured lateral absorbances, $A(x) = \ln(I_0/I)_x$, was fitted with a Gaussian function which was then Abel-inverted to obtain the local absorption coefficients. The effective absorption length was found to be about 0.6 mm.

The cavity length was chosen to be 0.67 m. The empty cavity provides a theoretical ring-down time up to 6 μs, but laser instability, coupling of several laser modes, scattering, and degradation of the mirrors reduce the observed empty-cavity decay time to about 2 μs. This time corresponds to a mirror reflectivity of about 0.999, or equivalently 500 round trips of the light pulse inside the cavity during the 1/e decay. The laser output was spatially filtered to form a Gaussian-like beam using two plano-convex lenses and a 100 μm pinhole. Then it was focused inside the cavity to match the TEM_{00} mode of the cavity. The mode-matching optics were calculated using matrix optics[32] and implemented using plano-convex lenses of focal lengths 5, 10, and 50 cm.

Following the recommendations of Yalin et al.,[31] special attention was paid to the choice of cavity geometry. Because the nanosecond atmospheric pressure discharges are generated in preheated gas at 1000 K, the presence of large temperature gradients affects the refractive index of air and causes beam steering effects (the plasma acts like a lens). Spuler and Linne[33] calculated the beam-steering displacement of a Gaussian beam for different values of the cavity parameter, $g = 1 - L/r$, where L is the cavity length and r the radius of curvature of the two identical mirrors. On the basis of their calculations, a good compromise for our experimental conditions is to take $g = -0.34$ ($L = 0.67$ m, $r = 0.5$ m). This configuration provides a small beam waist (fwhm = 0.4 mm), while maintaining a low sensitivity to beam steering effects. Another important aspect was the effect of the laser line width on the measured densities. Yalin and Zare[34] showed that the measured integrated line absorption coefficient is not conserved when the laser width is larger or comparable with the absorption line width and the peak absorbance, $\ln(I_0/I)_{max}$, is larger or comparable with the cavity loss, $(1 - R)$. As a result, the measured density underestimates the actual density. On the basis of the curves provided in ref 34, our measurements of the integrated absorption coefficients were essentially independent of the laser spectral width. Only the largest peak absorbances led to slightly underestimated density values (a few percent).

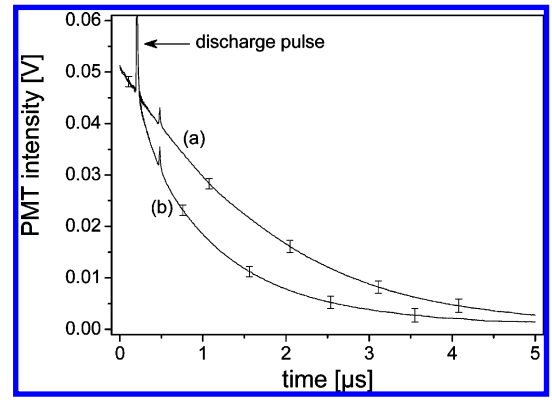

Figure 2. Typical measured ring-down signals in nitrogen. Curves a and b are recorded at $\lambda = 770.012$ nm (off-resonance) and $\lambda = 769.945$ nm (on-resonance), respectively.

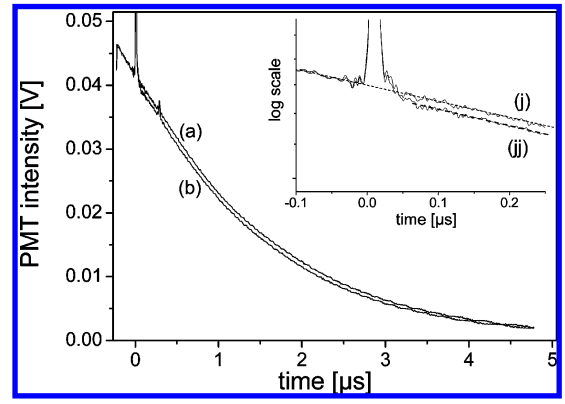

Figure 3. Typical measured ring-down signals in air. Curves a and b are recorded at the same wavelength as in Figure 2. The inset shows a zoom of curves a and b in log scale. The slopes (j) and (jj) are identical after 100 ns.

4. Results

4.1. Ring-Down Decays and Spectra Analysis. To obtain the time evolution of the species density, it is necessary in practice to measure the decay intensities with and without absorption. The function representing the time derivative of the logarithm of the ratio I_1/I_3 must be calculated (see eq 13). Finally the resulting function is directly proportional to the absorbing species density.

Typical CRDS signals in the nitrogen and air discharges are shown in Figures 2 and 3, respectively, where the decay curves a and b represent the decay functions I_1 and I_3, respectively. They were recorded off-resonance at $\lambda_{(a)} = 770.012$ nm and on-resonance at $\lambda_{(b)} = 769.945$ nm, respectively. The on-resonance wavelength corresponds to the unresolved $Q_1(22)$ and $Q_3(16)$ lines. These two lines could not be distinguished because their spacing of 4 pm (0.07 cm^{-1}) is smaller than the laser line width (~0.1 cm^{-1}).

The discharge pulse was delayed about 200 ns after the beginning of the ring-down decay. In Figure 2 the pulse corresponds to the first spike on the ring-down intensities. The first and subsequent spikes are due to the electromagnetic noise generated by the 10 ns high-voltage pulser. The data recorded during these spikes were not used in the analysis.

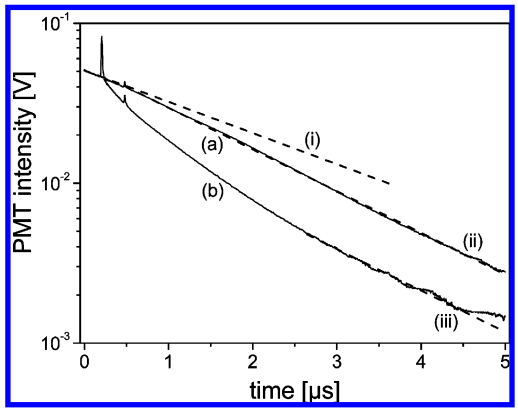

Figure 4. Ring-down signals from Figure 2 represented in log scale. The off- and on-resonance measurements are labeled curves a and b, respectively. Curve a is linear with slope I before the pulse and slope ii after the pulse. Curve b is identical to (a) before the pulse but has a nonlinear variation after the pulse, indicating changes of the $N_2(A)$ density in time. After 2.5 μs curves a and b become parallel (slope ii = slope iii).

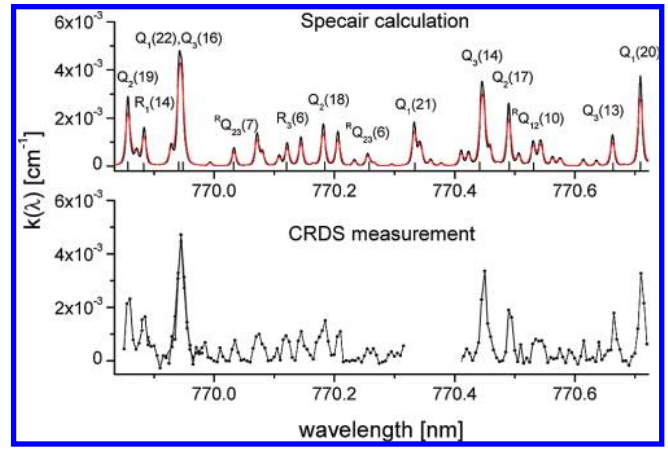

Figure 5. Comparison of the spectral absorption coefficient measured by CRDS and calculated by Specair. The simulated spectrum was obtained for $T_{trans} = T_{rot} = T_{vib} = 1600$ K, $[N_2(A)] = 2 \times 10^{14}$ cm^{-3}, and a 0.6 mm absorption length. In red is the spectrum convolved with the instrumental profile (Gaussian of fwhm = 0.1 cm^{-1}).

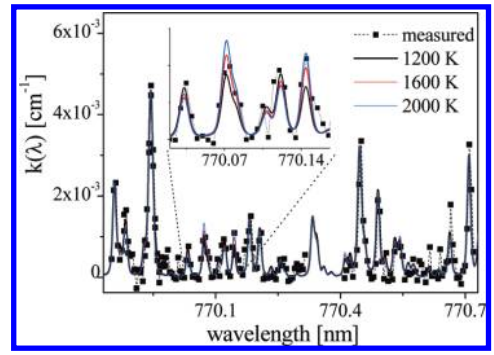

Figure 6. Measured CRDS spectra fitted for rotational temperatures of 1200, 1600, and 2000 K. The inset shows the lines that are most sensitive to the rotational temperature.

It should be noted that in the present experiments diffusion processes are negligible because the characteristic diffusion time (of the order of 100 μs) is much longer than the duration over which the present measurements were made (0−2 μs).

During the first 200 ns of the decay, the $N_2(A)$ density is negligible because the characteristic time of collisional quenching and pooling reactions is less than 1 μs,[8,14] and therefore the $N_2(A)$ produced by the previous pulses is expected to have disappeared. This explains why the on- and off-resonance curves (a, b) are identical before the pulse.

In Figure 4 the two ring-down signals from Figure 2 are represented in logarithmic scale. The data obtained in the 200 ns before the discharge pulse could be fitted and used to determine the off-resonance characteristic ring-down time (slope i). However, as seen in Figure 4, the off-resonance decay rate changes after the pulse. This is shown by two curves: the slope (i) corresponding to the off-resonance decay before the discharge is smaller than the slope (ii) measured after the pulse. This change is attributed to temperature gradients (hence inducing a change of the refractive index). As a consequence the laser beam may *walk away* from the cavity. Because the beam-steering has negligible wavelength dependence over the small spectral region used, curves (a) and (b) have the same loss rate due to this effect. By inspection of eq 13, it is clear that these effects cancel out in the resulting $N_2(A)$ density. Another important parameter that affects the decay rate is the reflectivity of the mirrors. However their reflectivity is constant over the spectral domain used because the decays obtained for the on- and off-resonance curves (a, b) are identical before the discharge pulse. Other laser beam losses such as plasma scattering (Thomson and Rayleigh scattering) are negligible compared to absorption or mirror losses.

Contrary to the off-resonance ring-down signal, the logarithm of the on-resonance signal does not vary linearly. This indicates that the density of $N_2(A)$ changes during the ring-down time. We also see in Figure 4 that the slope iii of the on-resonance decay starting at about $t = 2.5$ μs is the same as the off-resonance slope ii. This indicates that absorption by $N_2(A)$ becomes too small to be measured after 2.5 μs.

The absorption coefficients of the first positive nitrogen system in nonequilibrium air and nitrogen plasmas were computed using the line-by-line radiation code SPECAIR.[35] In this code, the line strengths are calculated using transition probabilities from Laux et al.,[36] which are based on the ab initio electronic transition moment functions of Werner et al.[37] The quoted accuracy of the resulting transition probabilities of the first negative system is 10% (ref 36). Next the Voigt profile functions are calculated as a convolution of natural, Doppler, van der Waals, resonance, and instrumental broadening. Finally, the absorption coefficients are obtained using eq 5 and are compared with the measured spectrum.

Figure 5 shows the CRDS spectrum measured in nitrogen, along with a fitted synthetic spectrum simulated with SPECAIR.[35] The experimental CRDS spectrum corresponds to the average $N_2(A)$ density over the 500 ns following the discharge pulse and was measured with a 5 pm spectral step. The simulated spectrum is obtained for $T_{trans} = T_{rot} = T_{vib} = 1600$ K, $N_2(A)$ density of 2×10^{14} cm^{-3}, and a 0.6 mm absorption length. The curve in red corresponds to the simulated spectrum convolved with the instrumental function, which for our laser system is a Gaussian with fwhm = 0.1 cm^{-1}. Laser broadening reduces the absorption coefficient of the spectral peaks, for instance, by about 7% at 769.945 nm.

4.2. Temperature Measurements. The $N_2(A)$ density obtained from the measured rotationally resolved spectrum is sensitive to the translational, rotational, and vibrational temperatures. Thus the temperature values are very important for accurate measurement of the metastable density.

In Figure 6 the spectrum from Figure 5 was fitted for rotational temperatures of 1200, 1600, and 2000 K. The inset shows a zoom of the spectrum containing the lines that are the most sensitive to the rotational temperature. The best fit is

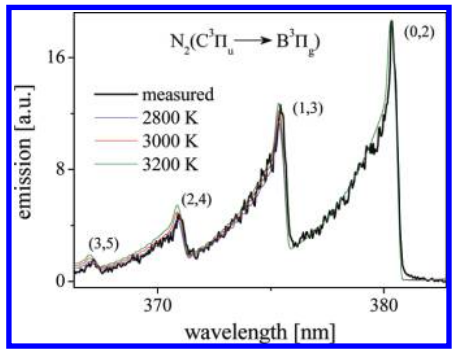

Figure 7. Measured optical emission spectra of the second positive system of N_2 and fit obtained with $T_{rot} = 1600$ K and $T_{vib} = 2800$, 3000, and 3200 K.

obtained for a rotational temperature of 1600 (±300) K. We emphasize here that this is an average temperature for the 500 ns postdischarge period. The translational temperature was considered to be in equilibrium with the rotational temperature because at atmospheric pressure the translational−rotational relaxation is a very fast process (a few nanoseconds).[38] Unfortunately the vibrational temperature could not be measured because the spectral region accessible to the CRDS system only contains lines of a single vibrational band, the (2 ← 0) vibrational band. For the spectral fit, the vibrational temperature was assumed to be also in equilibrium with the gas temperature during the postdischarge measurements. This assumption is not always true. However, an estimate of the vibrational temperature can be obtained from the relative intensities of vibrational bands of the second positive system of N_2, which were measured by OES.

Figure 7 shows the emission spectrum of the second positive system of N_2 measured during the 10 ns discharge. SPECAIR was used to fit the rotational structure of the (0 → 2) vibrational band. The best fit is obtained for a rotational temperature of 1600 (±200) K. The vibrational temperature is obtained from the fit of the vibrational bands (0,2), (1,3), (2,4), and (3,5). The spectrum is fitted for vibrational temperatures of 2800, 3000, and 3200 K, and the best fit is obtained for 3000 (±200) K. Compared to our earlier assumption of a vibrational temperature of 1600 K, the calculated absorption coefficients decrease only by 25%. Because the decays are measured in the postdischarge, the vibrational relaxation processes reduce the vibrational temperature. Especially for air plasmas with large atomic oxygen densities, vibrational−translational (VT) energy transfer occurs within microseconds.[38] Thus in the present analysis we consider that 3000 K is an upper limit for the vibrational temperature in the postdischarge. Accordingly, a total uncertainty of 40% was taken into account for the $N_2(A)$ density measurements.

4.3. Discharge in Nitrogen. Figure 8 presents the temporal evolution of the $N_2(A)$ density in the nitrogen discharge. This profile was obtained using eq 13 from an average of 100 on-resonance decay traces at 769.945 nm (which is the peak of strongest absorption line in the spectral range accessible to the present experiment) and an average of 100 off-resonance decay traces at 770.012 nm. Instead of taking the derivative of the logarithm of the ratio I_1/I_3, we fitted $\ln(I_1/I_3)$ with a 6th order polynomial function before calculating its derivative. This procedure considerably reduces numerical noise; however, data oscillation are generated.

Figure 9 shows the logarithm of the ratio I_1/I_3 together with the polynomial fit. It can be seen that about 2.5 μs after the discharge pulse $\ln(I_1/I_2)$ becomes constant. This means that the metastable absorption becomes negligible after this period of

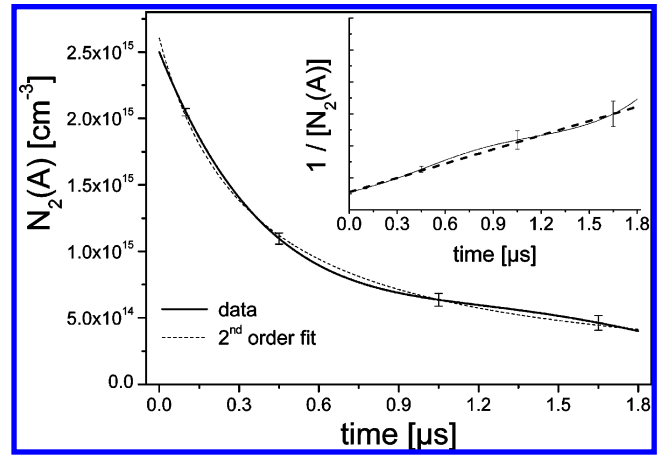

Figure 8. Time evolution of the $N_2(A)$ density in nitrogen plasma fitted by eq 15. The inset shows the reciprocal of $N_2(A)$ density fitted by eq 16. The data oscillations are due to the polynomial fit of $\ln(I_1/I_3)$.

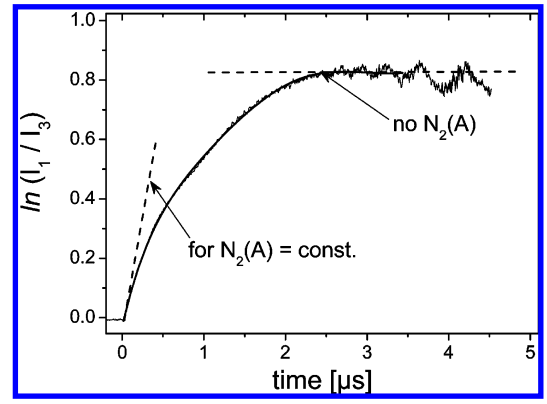

Figure 9. Time dependence of $\ln(I_1/I_3)$ fitted with a 6th order polynomial. The dashed horizontal line (I_1/I_3 = constant) corresponds to no $N_2(A)$ absorption. The tangent at the origin (dashed line) would correspond to constant $N_2(A)$ absorption.

time. Hence in the data treatment only the first 2 μs were used. The inclined dashed line is obtained for an arbitrary constant $N_2(A)$ density. In contrast the measured data from Figure 9 proves the $N_2(A)$ time variation.

From Figure 8 it can be seen that the $N_2(A)$ density increases to 2.5×10^{15} cm^{-3} immediately after the pulse and then decays with a characteristic time (N/e) of about 600 ns. During the discharge pulse and the 50 ns following it, no density measurements could be made because of the large EM noise that overlaps the decay signals. Contrary to classical CRDS experiments (i.e., for constant absorption) where the amplitude of the laser pulse does not influence the measurements of decay times, here the sensitivity depends on the pulse-to-pulse laser fluctuations. This is because the density is a function of the time derivative of $\ln(I_1/I_3)$. For the same reason the time resolution is also limited by laser intensity fluctuations. Additional fluctuations caused by the discharge limit the detection sensitivity and temporal resolution. Here the limit of detection was found to be 1 ppm for the 0.6 mm absorption length. And since at least two data points are needed to calculate the time derivative, the theoretical limit on temporal resolution corresponds to a round-trip duration (i.e., 5 ns) of the laser inside the cavity. Scattering of measured intensities limits our resolution to 20−50 ns depending on the signal-to-noise ratio of the ring-down intensity. To improve the sensitivity and temporal resolution, spectrally narrow continuous wave lasers (very small

intensity fluctuations) that excite only a single longitudinal mode of the cavity and higher reflectivity windows should be used.

The formation of electronically excited molecular nitrogen, e.g., $N_2(A)$, $N_2(B)$, $N_2(C)$, during the 10 ns pulse in atmospheric pressure nitrogen, occurs mainly via direct electron impact excitation. From emission spectroscopy measurements of the second and first positive systems of N_2, we have obtained the temporal evolution of the densities of $N_2(C)$ and $N_2(B)$ species.[39] The densities of these two electronic states decay with 1/e lifetimes of about 5−6 ns, whereas the radiative lifetimes are about 40 ns and 6 μs, respectively. These very short lifetimes are attributed to quenching by ground state nitrogen. Note however that $N_2(A)$ has a much longer lifetime (600 ns).

Because the $N_2(A)$ measurements are made about 50 ns after the pulse, only the decay phase of the metastable density is recorded. The densities of $N_2(B)$ and $N_2(C)$ were measured only in the first 20 ns after the pulse, because their decay is very fast. Thus, the reaction channels forming $N_2(B)$, $N_2(C)$ via pooling could not be investigated here, as for instance in refs 5, 6, and 12

If the main loss channel of the metastable is via the energy pooling reactions (R2) then the rate equation for the metastable density, N, is given by

$$\frac{dN}{dt} = -k_2 N^2 \tag{14}$$

The metastable density decay should be controlled by a second-order process, and thus its measurement should be well fitted by the function

$$N(t) = \frac{N_0}{N_0 k_2 t + 1} \tag{15}$$

where N_0 is the density at $t = 0$. The reciprocal of $N(t)$ should thus have a linear dependence on time

$$\frac{1}{N(t)} = \frac{1}{N_0} + k_2 t \tag{16}$$

with a slope equal to the pooling rate coefficient.

The data from Figure 8 were fitted using eq 15. The inset in Figure 8 shows that $1/N$ is well fitted by a linear curve. The slope gives a pooling rate coefficient $k_2 = 1.1 \times 10^{-9}$ cm^3 s^{-1} at the gas temperature of 1600 K. To our knowledge the pooling rate at 1600 K has not been measured. However, if we assume that the pooling rate coefficient varies as $T^{1/2}$ (as shown in ref 8 for the quenching rate by O_2), the inferred value at room temperature is about 5×10^{-10} cm^3 s^{-1}. As will be seen below, this is in good agreement with the values at $T = 300$ K reported in the literature.

Following Stedman et al.[12] who measured the pooling rate for $N_2(C)$ production, Hays et al.[13] measured a total pooling rate of $k_2 = 2(1.4 \times 10^{-9}$ cm^{3}s$^{-1})$. Nadler et al.[14] identified the channels of the pooling reactions at room temperature and found also the highest rate coefficient, k_B, for the production of $N_2(B)$, about $0.22k_B$ for the production of $N_2(C)$, $0.02k_B$ for the production of $N_2(C')$, and $0.03k_B$ for the production of N_2(HIR), with a total pooling rate $k_2 = 2(k_B + k_C + k_{C'} + k_{HIR}) = 3 \times 10^{-9}$ cm^3 s^{-1}, with a reported uncertainty of a factor 2−3. A few years later, Piper[15,16] also investigated the pooling channels and reported a lower limit for the total pooling rate of $(0.3-0.5) \times 10^{-9}$ cm^{3}s^{-1}. Thus the reported values of the total pooling rate coefficient at $T = 300$ K vary from 0.3 to 3×10^{-9} cm^3 s^{-1}. This wide range of values is explained by uncertainties on the reaction channels of the metastable.

Other important loss channels of $N_2(A)$ in nitrogen plasmas include quenching by atomic nitrogen[23,40]

$$N_2(A) + N \rightarrow N_2(X) + N \tag{R3}$$

and the production of $N_2(B)$ from the reaction[6,41]

$$N_2(A) + N_2(X, v > 5) \rightarrow N_2(B) + N_2(X, v - 6) \tag{R4}$$

Both reactions are single order processes. Therefore, since Figure 8 clearly shows that the decay is a second-order process, we conclude that (R3) and (R4) are much slower than the pooling reaction (R2). It follows that $k_3[N] \ll k_2[N_2(A)]$ and $k_4[N_2(X, v > 5)] \ll k_2[N_2(A)]$, where k_3 and k_4 stand for the rate coefficients of reactions (R3) and (R4), with $k_3 = 5 \times 10^{-11}$ cm^3 s^{-1} from ref 40 and $k_4 = 3 \times 10^{-11}$ cm^3 s^{-1} from ref 41. On the basis of these rate coefficients and the measured $N_2(A)$ density, we conclude that the mole fractions of N and $N_2(X, v > 5)$ are <1% in our discharge. Other losses through diffusion are also negligible in our experiment because the decay time of the metastable density is much shorter than the characteristic diffusion time.

In our experiments, we believe that the main uncertainties come from the repopulation of $N_2(A)$ by quenching of N_2* higher electronically excited states in collision with $N_2(X)$, N, and possibly by O_2 impurities. Additional uncertainties for temperatures and densities were considered. Thus we estimate that the measured total pooling rate coefficient at 1600 K is 1.1×10^{-9} cm^3 s^{-1}, with a factor of 2 uncertainty, which includes as well 40% for density and 15% for temperature uncertainties.

4.4. Discharge in Air. The decay curves shown in Figure 3 were recorded on- and off-resonance, and each represents an average of 100 decays. They were obtained with dry air under the same discharge and temperature condition as for the case of nitrogen. The inset in Figure 3 shows the decay curves in logarithmic scale. It can be seen that after about 100 ns the intensity decay rates are identical, i.e., they have the same slope: (j) and (jj), respectively. Thus there is no detectable density of the $N_2(A)$ metastable after ~100 ns. The average density during the first 100 ns following the pulse is obtained to be 5×10^{14} cm^{-3} using the relation

$$N_{average} = \frac{1}{S(T)\phi(\nu)} \frac{L}{c l_{abs}} \frac{\ln(I_1/I_3)_{t=100ns} - \ln(1)}{\Delta t} \tag{17}$$

where $\Delta t = 100$ ns. The on- and off-resonance decay rates are too noisy to obtain time evolution data, but clearly the lifetime is shorter than 100 ns, about 1 order of magnitude shorter than in the nitrogen discharge. Thus the main depletion mechanism in air is not pooling. Instead we expect depletion to occur mainly through quenching by O_2, O, NO, or other species.

If the discharge does not significantly dissociate O_2, then this species should be the main quencher of the metastable. Several measurements of the rate coefficient of $N_2(A)$ quenching by molecular oxygen at room temperature[8,11,42,43] have been reported, with values ranging from $k_1 = 1.6$ to 2.9×10^{-12} cm^3 s^{-1}. To our knowledge there are no data published for $T = 1600$ K, but de Sousa et al.[8] have shown a $T^{1/2}$ dependency of the quenching rate coefficient of the metastable in $v = 0$ (our measured transitions are from this level) in the temperature range 80−560 K.

If we apply the $T^{1/2}$ dependence to the literature values up to 1600 K, and if we assume that oxygen is not dissociated, then the quenching rate is about 6×10^{-12} cm^3 s^{-1}, corresponding to a lifetime ($t_{N_2A} = 1/k_1 N_{O_2}$) of about 250 ns. This lifetime is

slightly higher than the measured value of less than 100 ns. The presence of important quantities of faster quenchers such O (3×10^{-11} cm^3 s^{-1} refs 11, 44, and 45), N (5×10^{-11} cm^3 s^{-1} ref 40), and NO (about 1.1×10^{-10} cm^3 s^{-1} refs 11 and 46) could explain the shorter measured lifetime. Using TALIF,[47] we have recently found that the pulsed discharge in air, for the same conditions as reported here, can dissociate molecular oxygen up to 50%. With the O quenching rate coefficient of 3×10^{-11} cm^3 s^{-1} mentioned above, the resulting lifetime should be 20−30 ns. Thus, the $N_2(A)$ lifetime observed here is consistent with fast quenching by atomic oxygen.

5. Conclusions

Pulsed CRDS has proven to be a suitable technique to measure the absolute density of $N_2(A)$ with high temporal (50 ns) resolution, even in the hostile environment of atmospheric pressure NRP discharges where high-temperature gradients, small volumes, fast quenching processes, and high electromagnetic noise make the measurements challenging.

The gas temperature was obtained from the rotationally resolved CRDS spectrum. The temperature was shown to be the same as the rotational temperature obtained from the emission spectra of the second positive system of N_2.

The results presented here indicate that the characteristic lifetime of the metastable is about 600 ns in nitrogen at 1600 K and 1 atm, and less than 100 ns in air under the same conditions of temperature and pressure. In nitrogen, the main depletion process of the metastable is the energy pooling, whereas in dry air, the main process is quenching by O and O_2. We measured a pooling rate coefficient at 1600 K of 1.1×10^{-9} cm^3 s^{-1} (with a factor 2 uncertainty), in good agreement with the literature.

Acknowledgment. This work was supported by a Chaire d'Excellence awarded by the Ministère de l'Enseignement Supérieur et de la Recherche, by the ANR (Agence Nationale de la Recherche) under the IPER program (Grant Number ANR-05-BLAN-0090), and by Région Ile-de-France. We would also like to thank T. G. Spence and C. Harb for their help with the CRDS software and technical advice.

References and Notes

(1) Becker, K. H.; Kogelschatz, U.; Schoenbach, K. H.; Barker R. J., *Non-equilibrium Air Plasmas at Atmospheric Pressure*; IOP Publishing: Bristol, U.K.,2004ISBN 0750309628.
(2) Kruger, C. H.; Laux, C. O.; Yu, L.; Packan, D. M.; Pierrot, L. *Pure Appl. Chem.* **2002**, *74* (3), 337.
(3) Machala, Z.; Laux, C. O.; Kruger, C. H. *IEEE Trans. Plasma Sci.* **2005**, *33*, 2–320.
(4) Pai, D. , PhD thesis, Ecole Centrale Paris, France, 2008.
(5) Cartry, G.; Magne, L.; Cernogora, G. *J. Phys. D: Appl. Phys.* **1999**, *32*, 1894.
(6) Gatilova, L. V.; Allegraud, K.; Guillon, J.; Ionikh, Y. Z.; Cartry, G.; Roepcke, J.; Rousseau, A. *Plasma Sources Sci. Technol.* **2007**, *16*, S107.
(7) Clark, W. G.; Setser, D. W. *J. Phys. Chem.* **1980**, *84*, 2225.
(8) De Sousa, A. R.; Touzeau, M.; Petitdidier, M. *Chem. Phys. Lett.* **1985**, *121*, 423.
(9) Ho, G. H.; Golde, M. F. *J. Chem. Phys.* **1991**, *95* (12), 8866.
(10) Tao, W.; Golde, M. F.; Ho, G. H. *J. Chem. Phys.* **1992**, *96* (1), 356.
(11) De Benedictis, S.; Dilecce, G. *J. Chem. Phys.* **1997**, *107* (16), 6219.
(12) Stedman, D. H.; Setser, D. W. *J. Chem. Phys.* **1969**, *50*, 2256.
(13) Hays, G. N.,; Oskam, H. J. *J. Chem. Phys.* **1973**, *59*, 1507.
(14) Nadler, I.; Rosenwaks, S. *J. Chem. Phys.* **1985**, *83* (8), 3932.
(15) Piper, L. G. *J. Chem. Phys.* **1988**, *88* (1), 231.
(16) Piper, L. G. *J. Chem. Phys.* **1988**, *88* (1), 6911.
(17) Pilla, G.; Galley, D.; Lacoste, D. A.; Lacas, F.; Veynante, D.; Laux, C. O. *IEEE Trans. Plasma Sci.* **2006**, *34* (6), 2471.
(18) Pilla, G. PhD thesis, Ecole Centrale Paris, France, 2008.
(19) Cook, J. M.; Miller, T. A.; Bondybey, V. E. *J. Chem. Phys.* **1978**, *69* (6), 2562.
(20) De Benedictis, S.; Dilecce, G.; Simek, M. *J. Phys. D: Appl. Phys.* **1998**, *31*, 1197.
(21) Dilecce, G.; Ambrico, P. F.; De Benedictis, S. *Plasma Source Sci. Technol.* **2007**, *16*, 511.
(22) Hadj Bachir, I.; Huet, T. R.; Destombes, J. L.; Vervloet, M. *Chem. Phys. Lett.* **1997**, *270*, 533.
(23) Cernogora, G.; Ferreira, C. M.; Hochard, L.; Touzeau, M.; Loureiro, J. *J. Phys. B: At. Mol. Phys.* **1984**, *17*, 4429.
(24) Scripter, C.; Augustyniak, E.; Borysow, J. *Chem. Phys. Lett.* **1993**, *201*, 194.
(25) Augustyniak, E.; Borysow, J. *J. Phys. D: Appl. Phys.* **1994**, *27*, 652.
(26) *Cavity ringdown spectroscopy. an ultratrace absorption measurement technique*; Busch, K. W., Busch, M. A., Eds.; ACS symposium series 720, American Chemical Society: Washington, DC, 1999; DOI 10.1021/bk-1999-0720.
(27) Yalin, A. P.; Laux, C. O.; Kruger, C. H.; Zare, R. N. *Plasma Source Sci. Technol.* **2002**, *11*, 248.
(28) Gupta, M.; Owano, T.; Baer, D.; Keefe, A. O. *Appl. Phys. Lett.* **2006**, *89*, 241503.
(29) Gupta, M.; Owano, T.; Baer, D.; Keefe, A. O.; Williams, S. *Chem. Phys. Lett.* **2004**, *400*, 42.
(30) Brown, S. S.; Ravishankara, A. R.; Stark, H. *J. Phys. Chem. A* **2000**, *104*, 7044.
(31) Yalin, A. P.; Zare, R. N.; Laux, C. O.; Kruger, C. H. *Appl. Phys. Lett.* **2002**, *81*, 8–1408.
(32) Kogelnik, H.; Li, T. *Appl. Opt.* **1966**, *5*, 10–1550.
(33) Spuler, S.; Linne, M. *Appl. Opt.* **2002**, *41*, 15–2858.
(34) Yalin, A. P.; Zare, R. N. *Laser Phys.* **2002**, *12*, 8–1065.
(35) Laux, C. O.; Spence, T. G.; Kruger, C. H.; Zare, R. N. *Plasma Sources Sci. Technol.* **2003**, *12*, 125.
(36) Laux, C. O.; Kruger, C. H. *J. Quant. Spectrosc. Radiat. Transfer* **1992**, *48*, 9.
(37) Werner, H. J.; Kalcher, J.; Reinsch, E. A. *J. Chem. Phys.* **1984**, *81*, 2420.
(38) Capitelli, M. ; Ferreira, C. M. ; Gordiets, B. F. ; Osipov, A. I. *Plasma Kinetics in Atmospheric Gases*; Springer: Berlin and New York, 2000.
(39) Stancu, G. D.; Kaddouri, F.; Lacoste, D. A.; Laux, C. O. *Workshop on Frontiers on Low Temperature Plasma Diagnostics, 8th*, Blansko, Czech Republic, 2009.
(40) Young, R. A.; St. John, G. A. *J. Chem. Phys.* **1968**, *48*, 895.
(41) Piper, L. G. *J. Chem. Phys.* **1989**, *91*, 864.
(42) Dreyer, J. W.; Perner, D.; Roy, C. R. *J. Chem. Phys.* **1974**, *61*, 3164.
(43) Piper, L. G.; Caledonia, G. E.; Kennealy, J. P. *J. Chem. Phys.* **1981**, *74*, 2888.
(44) Piper, L. G.; Caledonia, G. E.; Kennealy, J. P. *J. Chem. Phys.* **1981**, *75*, 2847.
(45) Thomas, J. M.; Kaufman, F. *J. Chem. Phys.* **1985**, *83*, 2900.
(46) Piper, L. G.; Cowles, L. M.; Rawlins, W. T. *J. Chem. Phys.* **1986**, *85*, 3369.
(47) Stancu, G. D.; Kaddouri, F.; Lacoste, D. A.; Laux, C. O. *AIAA, Plasmadynamics and Laser Conference, 40th*, San Antonio, TX, 2009; p 3593.

JP9075383